Efficient heat integration within discretely heat integrated distillation columns using liquid injection

Cui, Chengtian; van Reisen, Jos; Tyraskis, Ioannis; Kiss, Anton A.

DOI
10.1002/aic.18861

Publication date
2025

Document Version
Final published version

Published in
AIChE Journal

Received: 8 February 2025 | Revised: 16 March 2025 | Accepted: 2 April 2025

DOI: 10.1002/aic.18861

AIChE JOURNAL

RESEARCH ARTICLE

Process Systems Engineering

Efficient heat integration within discretely heat integrated distillation columns using liquid injection

Chengtian Cui[1] | Jos van Reisen[2] | Ioannis Tyraskis[3] | Anton A. Kiss[1]

[1]Department of Chemical Engineering, Delft University of Technology, Delft, The Netherlands

[2]McDermott, Den Haag, The Netherlands

[3]Energy & Materials Transition, TNO, Petten, The Netherlands

Correspondence
Anton A. Kiss, Department of Chemical Engineering, Delft University of Technology, Van der Maasweg 9, 2629 HZ, Delft, The Netherlands.
Email: a.a.kiss@tudelft.nl

Funding information
Ministerie van Economische Zaken en Klimaat, Grant/Award Number: TIND23-03473469

Abstract

Electrification of distillation processes through discretely heat integrated distillation columns (D-HIDiC) is an effective approach to enhance energy efficiency and lower carbon emissions. For separating systems with high temperature lift, multi-stage compression and inter-stage cooling are necessary to link the high-pressure rectifier and low-pressure stripper. Traditionally, heat recovery employs pumparound loops, but this study introduces liquid injection as a more efficient and innovative alternative. Simulation results using methanol/water separation indicate that liquid injection reduces both reboiler duty and compression power, achieving up to 50% primary energy savings compared with conventional distillation columns. Unlike continuous heat exchange in conventional HIDiC (C-HIDiC), D-HIDiC simplifies heat integration, avoiding complex hardware and energy penalties. Comparative analysis across multiple configurations, including SuperHIDiC, confirms the potential of D-HIDiC with liquid injection to fully electrify distillation, eliminate steam utility, and significantly support sustainable industrial operations.

KEYWORDS
column grand composite curve, discretely heat integrated distillation column, liquid injection, multi-stage compression, process electrification

1 | INTRODUCTION

Distillation is the most widely used unit operation for separation in the chemical process industries, accounting for 60% of the energy consumed across all separation technologies.[1] More specifically, it is responsible for about 40% of the energy use in the chemical industry, which accounts for about one third of the whole industrial sector.[2] In the context of sustainable development and environmental protection, shifting from fossil fuel-based processes to renewable-powered electrified systems is a pivotal step toward decarbonization and increased renewable energy integration.[3] In this regard, the electrification of distillation through heat pump assisted distillation (HPAD) has drawn much attention in recent years, as coupling process electrification with renewables-based low-carbon electricity offers a promising pathway for decarbonization.[4,5]

Compared with conventional distillation column (CDiC), HPAD has gained significant traction as a viable method for enhancing energy efficiency.[6] Various HPAD options have been proposed, but the most common one is vapor recompression (VRC).[7,8] In VRC, the overhead vapor is compressed to a higher pressure to serve as the heat source for the reboiler. However, the application of VRC is constrained to separations of close-boiling components, typically with boiling point differences (ΔT_b) within 20°C, such as C2 splitting ($\Delta T_b = 15.1$°C),[9,10] C3 splitting ($\Delta T_b = 5.5$°C),[11,12] and C4 splitting ($\Delta T_b = 11.2$°C).[12] This limitation arises because VRC must achieve a sufficient temperature lift (ΔT_{lift}) to cover the entire

column for effective heat exchange. Beyond conventional VRC setups, various modified processes, such as flash vapor circulation (FVC),[13,14] self-heat recuperation (SHR),[15] side-stream direct/reverse VRC,[16] and reduced vapor transfer structures with VRC,[17] have been introduced to further enhance process electrification. One notable HPAD advancement is the heat integrated distillation column (HIDiC), which operates by maintaining the rectifying and stripping sections of a distillation column at different pressures. This design facilitates heat exchange between sections, reducing the required temperature lift and compression ratio, thereby broadening the applicability of HPAD.[18]

HIDiC represents a breakthrough in improving energy efficiency of a heat pump design by maximizing internal heat integration. Unlike traditional VRC setups that rely on a single heat source (reboiler) and sink (condenser), HIDiC utilizes the entire high-pressure rectifying section as a heat source and low-pressure stripping section as a heat sink, thus substantially increasing the heat transfer area. For adjusting the pressures, a compressor and a throttling valve are installed between the two column sections. This design is commonly referred to as conventional HIDiC (C-HIDiC), as shown in Figure 1A. An alternative version without a condenser or reboiler is referred to as ideal HIDiC.[19] Although pilot-scale C-HIDiC designs have been explored in the Netherlands, commercial adoption has yet to be realized due to several practical limitations. For instance, De Rijke[20] conducted extensive experiments and simulations on concentric HIDiC designs, while Bruinsma et al.[21] tested plate-fin heat exchanger HIDiC designs. Later, Bruinsma et al.[22] introduced a plate-packing configuration with structured packing, which demonstrated improved performance over plate-fin heat exchanger HIDiC. Despite these advancements, C-HIDiC designs face inherent challenges, such as maintenance difficulties and constraints in optimizing internal heat exchange due to fixed wall or device positioning at the same elevation.

To improve energy efficiency in distillation processes, alongside evaluating various HIDiC configurations for internal heat integration, energy management in distillation preheat systems should also be considered to enhance external heat integration.[23] For instance, adding economizers can allow for the reuse of hot distillate and bottoms streams. In this context, Kansha et al.[24] utilized the SHR technique to improve heat recovery in a C-HIDiC, as depicted in Figure 1B. Beyond economizers, external condenser and reboiler integration, known as "different pressure thermally coupled distillation" (DPTCD)[25–27] is also possible, as illustrated in Figure 1C. This method can be viewed as a specialized form of HIDiC that incorporates a single heat exchanger.[3]

The world's first commercial application of HIDiC was proposed by Wakabayashi et al.[28] for separating a multicomponent mixture that mainly includes methyl-ethyl-ketone (light key, NBP = 79.6°C) and sec-butanol (heavy key, NBP = 99.5°C). With $\Delta T_b = 19.9$°C, the mixture remains within the 20°C limitation typically required for HPAD application. In this implementation, only a finite number of external heat exchangers were placed at specific points in the column sections, a design known as discretely HIDiC (D-HIDiC, Figure 1D).[29] In this work, we consider DPTCD as a specific D-HIDiC, as it shares the common characteristics of only a finite number of external heat exchangers. To design such a D-HIDiC, Wakabayashi and Hasebe[30] applied a modified Ponchon-Savarit *H-xy* and *T-xy* diagram design methodology, which was later extended to handle multicomponent systems.[31] Additionally, Harwardt and Marquardt[32] figured out that in the case of C-HIDiC, even when a sufficiently large heat transfer area is available, the energy savings achieved by integrating heat transfer

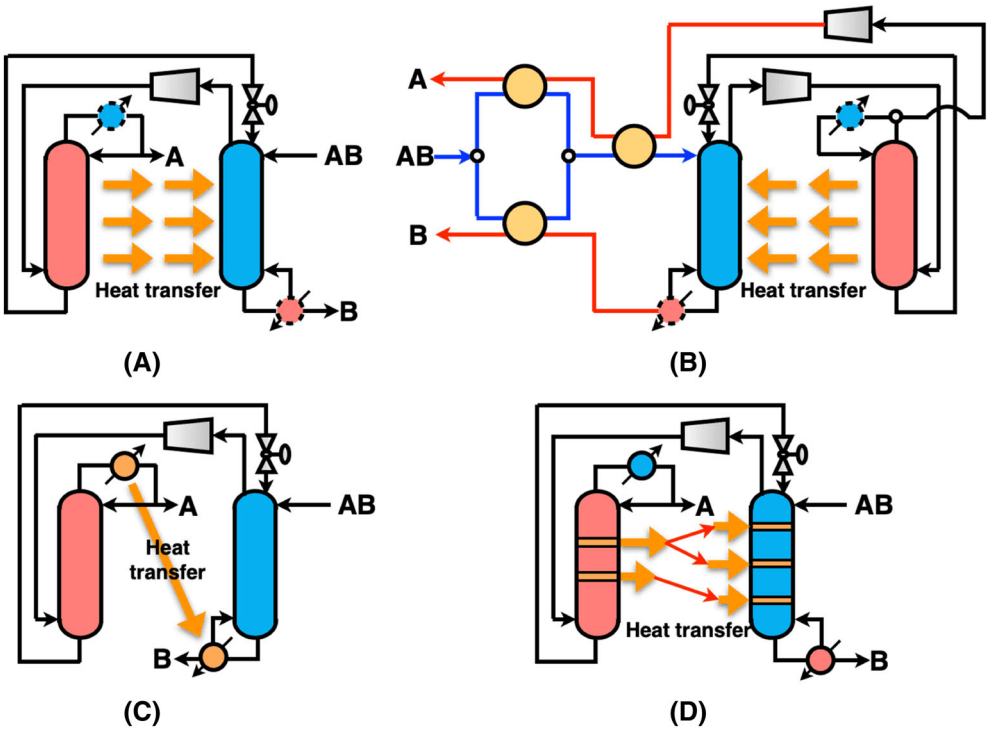

FIGURE 1 Process configurations for (A) C-HIDiC, (B) HIDiC-SHR, (C) DPTCD, and (D) D-HIDiC.

across each stage along the column height may only be minimal. However, implementing such designs requires specialized equipment to manage the extensive heat transfer areas, adding complexity without significant energy savings. Therefore, the main advantage of D-HIDiC lies in its minimalistic heat integration strategy, which suggests that a simpler setup with fewer heat exchangers can be economically beneficial compared with more complex configurations with numerous exchangers in a C-HIDiC.

The reviewed literature highlights the significant potential of D-HIDiC in advancing process electrification. However, the practical implementation of D-HIDiC systems remains highly challenging due to the inherent complexity associated with their design and optimization. Existing design methods, such as the one proposed by Wakabayashi et al.,[28] require complex graphical developments of *H-xy* and *T-xy* diagrams, limiting their practicality. To address these challenges, this study proposes an innovative yet straightforward design methodology for D-HIDiC using readily available models in Aspen Plus, eliminating the need for complex equilibrium diagrams and rigorous optimization.[33,34]

As a case study, we focus on methanol (NBP = 64.7°C)/water (NBP = 100°C) distillation, characterized by a large boiling point difference ($\Delta T_b = 35.3$°C). Notably, this exceeds the typical 20°C limit for HPAD. With a temperature driving force (ΔT_{df}) of 10°C, the $\Delta T_{lift} = \Delta T_b + \Delta T_{df} = 35.3$°C + 10°C = 45.3°C. To achieve such a significant temperature lift efficiently, a multi-stage compression strategy becomes essential. Previous HIDiC studies have predominantly focused on single-stage compression, often neglecting the substantial amount of intercooling duty required in multi-stage compression setups. Here, we not only introduce multi-stage compressors explicitly into the D-HIDiC design but also innovatively propose the use of liquid injection as a highly effective method for recovering intercooling duty. This novel approach contrasts with traditional methods relying on pumparound loops,[35] providing improved energy efficiency.

Furthermore, several new design variants of D-HIDiC employing liquid injection are introduced and evaluated. By demonstrating the effectiveness of liquid injection for intercooling heat recovery, this study significantly broadens the application scope of HIDiC technology, extending its applicability even to challenging separations with wider boiling point differences. Ultimately, this work contributes to the ongoing development of more efficient and versatile distillation processes suitable for industrial electrification efforts.

2 | PROBLEM STATEMENT AND MOTIVATION

This study introduces a novel design methodology for D-HIDiCs, exploring various heat integration strategies. Therefore, rigorous process optimization is beyond the scope of the present work. Motivated by the growing focus on process electrification, the aim is to operate the proposed D-HIDiC configurations without steam consumption during steady-state operation. The crude feed is an equimolar methanol/water mixture at 1 bar, closely resembling the methanol composition in the CO_2 hydrogenation process.[36,37] For comparison, traditional syngas-based methanol production often yields mixtures with higher methanol content, up to approximately 80 mol% methanol and 20 mol% water.[38] It is important to highlight that multi-effect distillation (MED),[39–41] while highly effective for impurity-rich mixtures (such as coal-based methanol), is not chosen as the benchmark in this study. The main reason is that direct CO_2 hydrogenation produces relatively pure methanol streams, containing primarily water and a minor amount of dissolved CO_2, thus making MED overly complex and unnecessary. Consequently, the CDiC serves as the benchmark case in our analysis, providing a more practical reference for evaluating the benefits of the proposed D-HIDiC configurations.

One of our key motivations for selecting methanol/water distillation as the case study is the anticipated deployment of e-methanol production facilities, as we expect the implementation of HIDiC is easier in these greenfield applications. Assuming an annual operating time of 8400 h, the capacity corresponds to 135 ktpy of methanol production. The product purities for methanol and water are both set at 99.99 mol%. For process simulation, the non-random two-liquid (NRTL) property model is used as a suitable model because of the presence of a non-ideal mixture containing polar components.

3 | DESIGN METHODOLOGY

The design methodology for D-HIDiC using Aspen Plus is briefly summarized in Figure 2, which is applicable to zeotropic mixtures. For the specified feed conditions, *Step 1* involves determining the benchmark steady-state design parameters for the CDiC, such as operating pressure, number of stages, and other key factors. These design parameters are determined through shortcut and rigorous design methods. For shortcut design, distillation with the Winn-Underwood-Gilliland *DSTWU* model is applied, while for rigorous design, the *RADFRAC* model is used in Aspen Plus. In *Step 2*, the rectifying and stripping column sections are split to make a preliminary D-HIDiC design. The operating pressure in the rectifying section is increased to achieve a sufficiently high temperature for effective heat transfer to the stripping section, resembling the well-proven air separation unit.[42,43] The column grand composite curve (CGCC), which is integrated into the *RADFRAC* model, serves as a useful tool for column energy targeting.[44] *Step 3* finalizes the D-HIDiC design based on the predetermined conditions, considering both internal and external heat integration.

3.1 | Design of CDiC as a benchmark

The benchmark CDiC is simulated using the *DSTWU* and *RADFRAC* models in Aspen Plus. The *DSTWU* model is used to estimate the minimum reflux ratio and the minimum number of stages, which serve as boundaries for designing a distillation column. The detailed shortcut design of CDiC can be viewed in the Data S1.

Based on the initial data from *DSTWU* simulation, the *RADFRAC* model is employed for rigorous distillation column design. Sulzer standard Mellapak 350Y is selected for the packed column internals due

to its high mass transfer efficiency, low pressure drop, and suitability for the column's geometric and operational requirements. Considering a HETP (Height Equivalent to a Theoretical Plate) of 0.5 m, a total height of 19 meters for 38 stages can be obtained. To account for factors beyond the packing height alone, such as liquid holdup for surge capacity, necessary net positive suction head requirements for pump, and so on, an additional 20% height oversizing is considered, as suggested by design heuristics.[45] Sensitivity analysis is applied to identify the optimum feed stage by minimizing reboiler duty. Figure 3 shows the benchmark CDiC designs under 1 bar and 5 bar operating pressures. Considering $\Delta T_{df} = 10^{\circ}C$, the high-pressure overhead vapor can be used to drive the low-pressure column reboiler. Although vacuum operation in the stripping section is also possible, we did not consider this case.[46] It can be observed that, with an increase in operating pressure, the high-pressure column uses ~20% more energy than the low-pressure column.

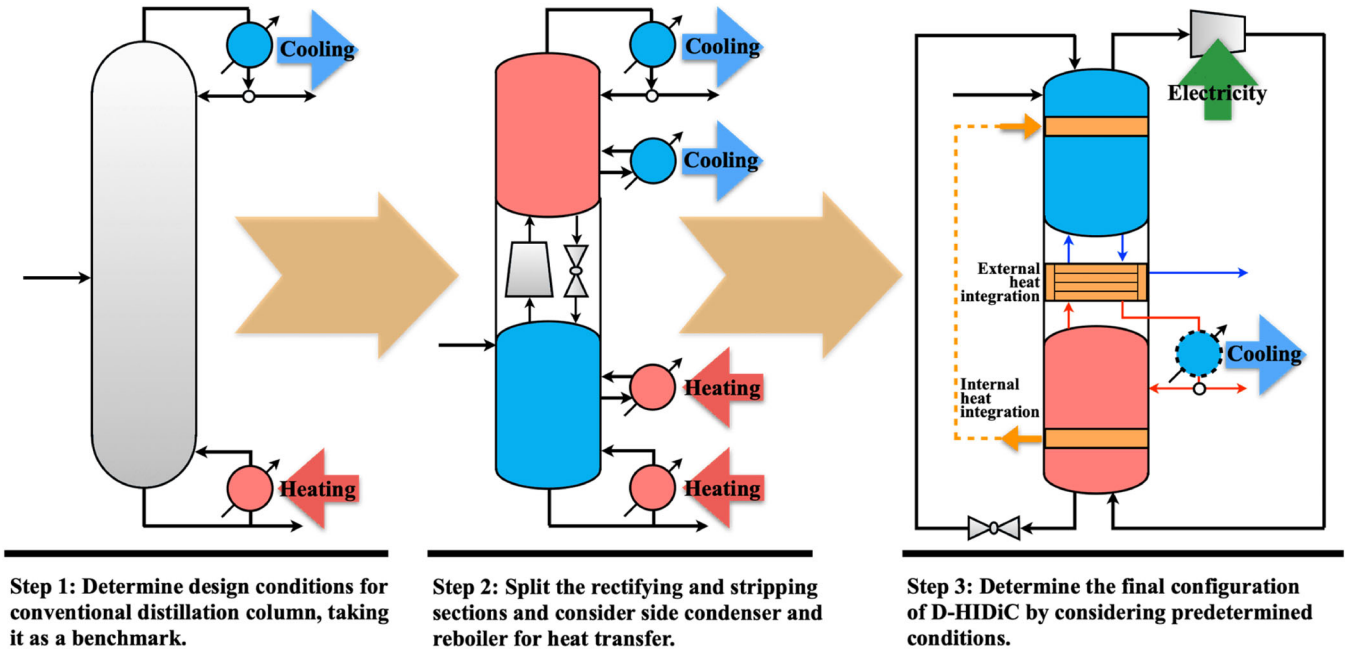

FIGURE 2 Design methodology for D-HIDiC.

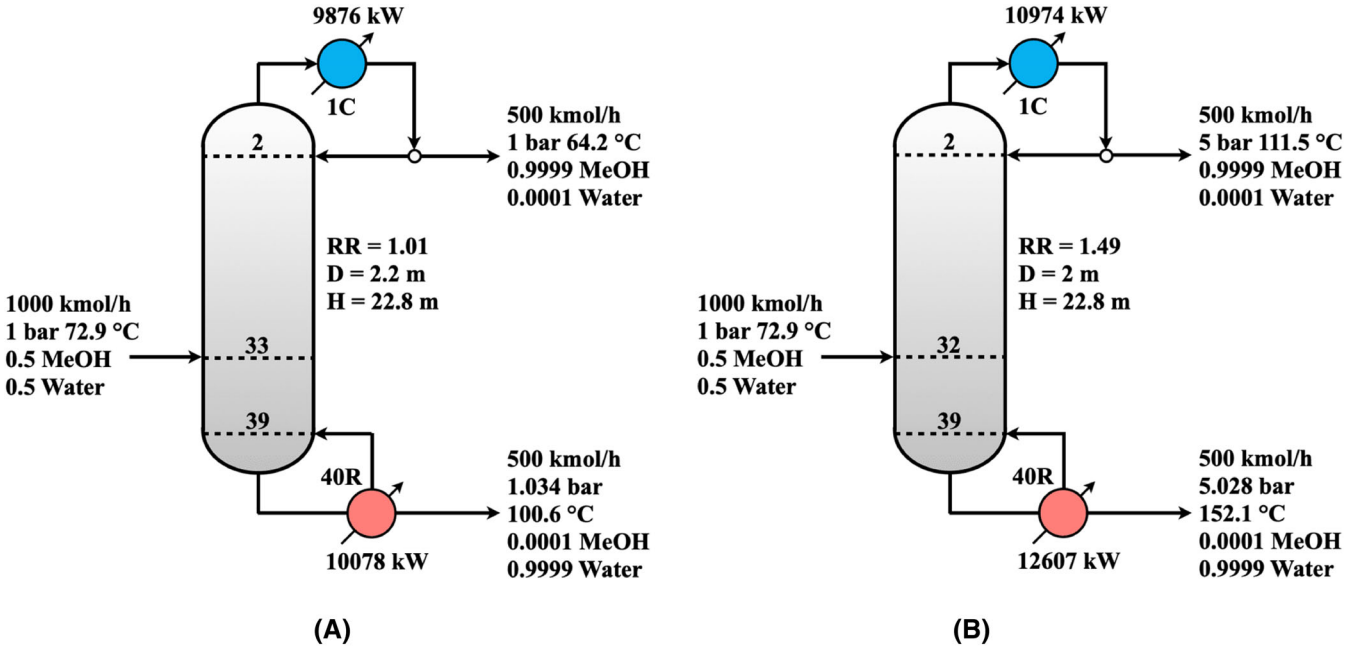

FIGURE 3 (A) Low-pressure CDiC and (B) high-pressure CDiC.

3.2 | Preliminary design of D-HIDiC

3.2.1 | Splitting the rectifying and stripping sections

In *Step 2*, based on the CDiC design in Figure 3, we begin by splitting the rectifying and stripping sections to operate at different pressures, linked by a compressor and a valve. Considering the optimum feed stage of the CDiC, the low-pressure stripping section is designed with 8 stages (Stage 33 to 40, including the reboiler), while the high-pressure rectifying section is set up with 32 stages (stage 1 to 32, including the condenser). In the preliminary design phase, a stage pressure drop of 0.007 bar is considered for conservative design.[45] It should be noted that if structured packing is used, the pressure drop could be lower. Under this large pressure drop, the impact of internal heat integration on the duty reduction in the main condenser and reboiler can be easily calculated, as given in the next section.

Figure 4 shows the Aspen Plus flowsheet for the D-HIDiC with independent condenser and reboiler. The reboiler duty is 10,413 kW, closely matching the 10,078 kW required in the low-pressure CDiC, and the condenser duty is 10,847 kW, slightly lower than the 10,974 kW in the high-pressure CDiC. The compression system compresses the overhead vapor from 1 bar (top pressure of the stripping section) to 5.217 bar (bottom pressure of the rectifying section). As the compression ratio is typically 2.5 to 4.0,[47] a two-stage compressor with inter-stage cooling is implemented, with the compressor's isentropic efficiency set to be 80%. The discharge temperature of each compression stage is limited to 175°C to meet compressor design standards.[48] Inter-stage cooling reduces the vapor temperature to 110°C, ~10°C superheating, which is sufficient to meet the compression discharge temperature requirement and avoid the use of the knock out drum.[49] The total compression power is 2037 kW, with an intercooling duty of 584 kW. As the intercooling temperature is higher than the temperature in the stripping section, this cooling duty can be recovered within the stripping column via traditional pump-around loops.[50]

An alternative approach to utilize the intercooling duty is to implement liquid injection, which is commonly used in refrigeration cycles to improve overall coefficient of performance (COP).[51,52] This liquid injection method is considered for the first time in this work to improve the efficiency of D-HIDiC, achieved by using a portion of the bottoms from the rectifying section, as illustrated in Figure 5. This way reduces the reboiler duty to 9961 kW while slightly increasing the condenser duty to 10,929 kW. This adjustment is beneficial, as it simplifies the heat integration of intercooling without requiring an additional heat exchanger in the column. Furthermore, the additional vapor traffic in the rectifier can supply more high-temperature condensation heat for heat exchange purposes. The compression power is reduced to 1987 kW, slightly lower than the original 2037 kW, due to a lower vapor flow rate passing through the first compressor.

3.2.2 | Addition of side condenser and side reboiler

For external heat integration, the reduction of the main condenser duty Q_C (all heat duties are in absolute value) and main reboiler duty Q_R depends on the amount of heat exchanged Q_E:

$$Q_C = Q_{C,0} - Q_E, \tag{1}$$

$$Q_R = Q_{R,0} - Q_E, \tag{2}$$

where $Q_{C,0}$ and $Q_{R,0}$ are the initial duties before heat integration.

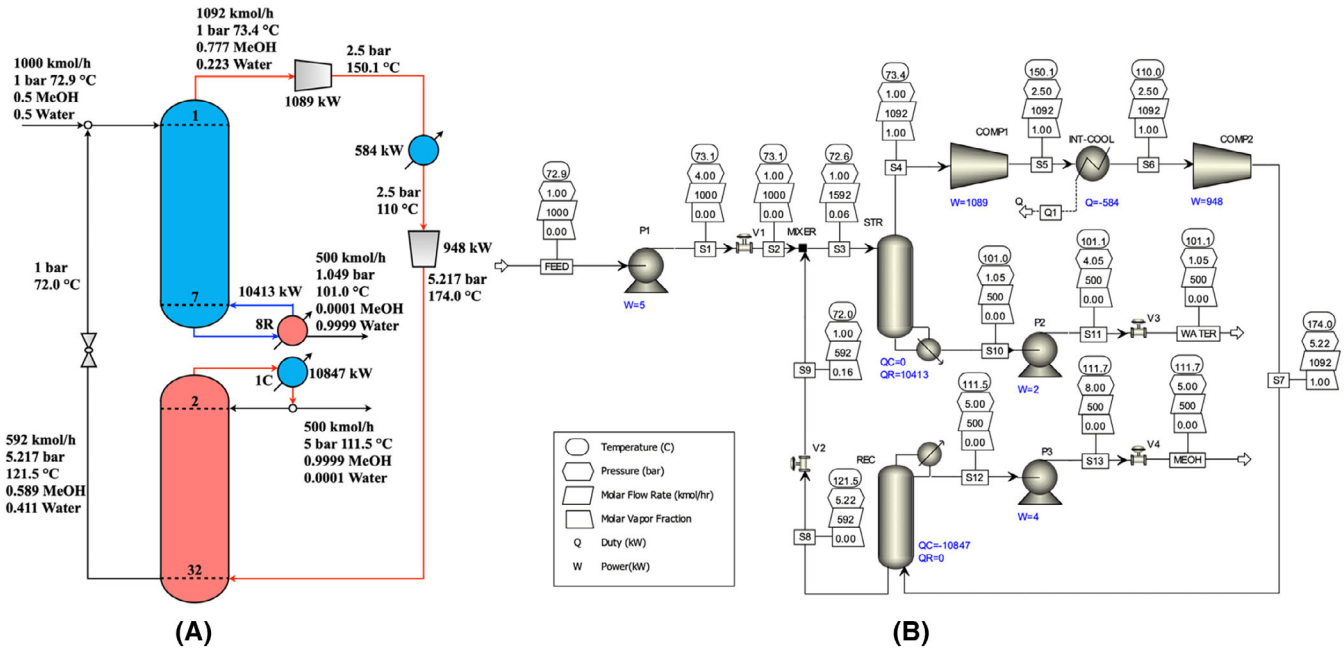

FIGURE 4 (A) Preliminary design of D-HIDiC; (B) Aspen Plus flowsheet for D-HIDiC with independent reboiler and condenser.

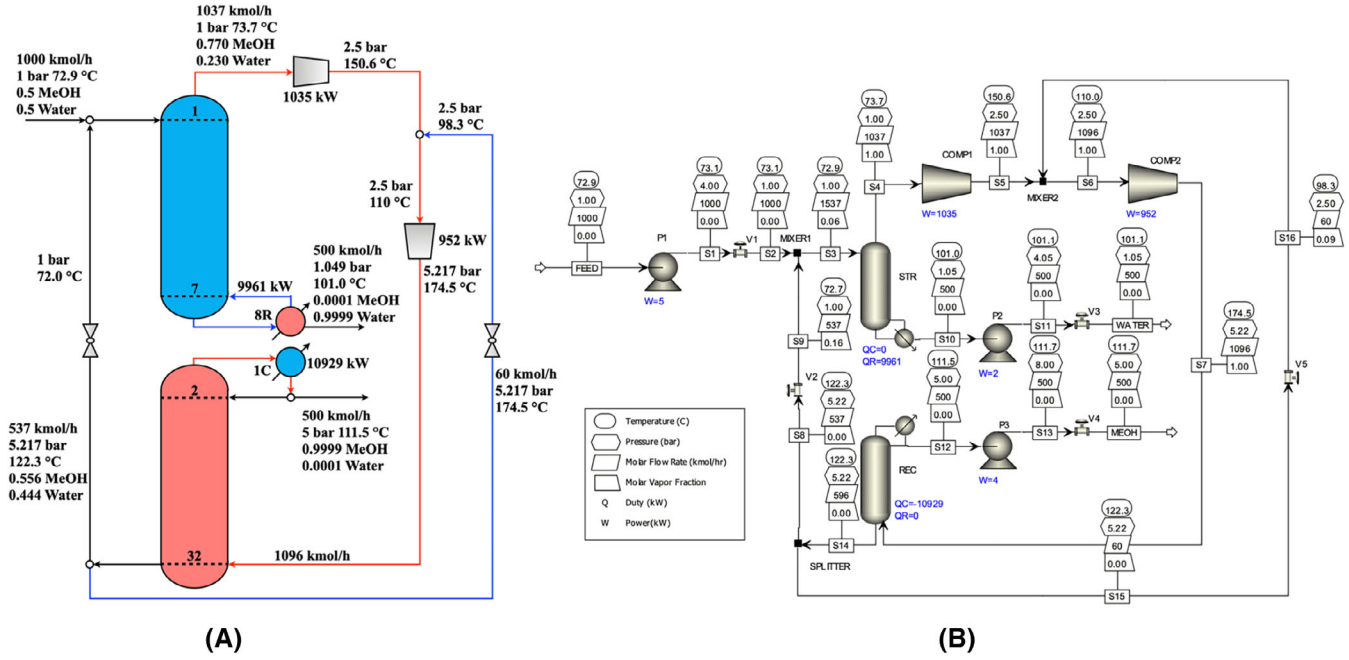

FIGURE 5 (A) Preliminary design of D-HIDiC with liquid injection; (B) Aspen Plus flowsheet for D-HIDiC with independent reboiler, condenser, and liquid injection.

However, the reduction of the main condenser and main reboiler duties through internal heat integration depends on two factors: (1) the location of the heat exchange stages and (2) the amount of heat exchanged. Normally, shifting some heat load from the main condenser to the side condenser or from the main reboiler to the side reboiler may introduce an energy penalty due to changes in separation driving forces.[53] Therefore:

$$Q_C > Q_{C,0} - Q_E, \tag{3}$$

$$Q_R > Q_{R,0} - Q_E. \tag{4}$$

To account for this, we introduce the factors $\varepsilon_{R,j}$ and $\varepsilon_{S,j}$, which represent the effective contribution ratios of stage heat duty for reducing condenser or reboiler duties. Here, subscripts R, S, and j denote the rectifying section, stripping section, and stage number, respectively:

$$Q_C = Q_{C,0} - \varepsilon_{R,j} Q_E, \tag{5}$$

$$Q_R = Q_{R,0} - \varepsilon_{S,j} Q_E. \tag{6}$$

Rearranging Equations (5) and (6), we can obtain:

$$\varepsilon_{R,j} = \frac{Q_{C,0} - Q_C}{Q_E} = \frac{\Delta Q_C}{Q_E}, \tag{7}$$

$$\varepsilon_{S,j} = \frac{Q_{R,0} - Q_R}{Q_E} = \frac{\Delta Q_R}{Q_E}. \tag{8}$$

These equations allow us to evaluate the effectiveness of side condensers and reboilers in distributing heat load, which impacts the duties of the main condenser and reboiler. In this work, the CGCC tool is used to identify the heat exchange stages and amount of heat to transfer, thereby enhancing the column overall efficiency. Based on the preliminary D-HIDiC design shown in Figure 4, Figure 6A illustrates the CGCC for the high-pressure rectifying section and the low-pressure stripping section. The enthalpy differences $\Delta H_{R,j}$ and $\Delta H_{S,j}$ at each stage are calculated from the CGCC results, as depicted in Figure 6B. For the stripping section, significant enthalpy differences are observed on stages S2 and S3, suggesting these stages as potential candidates for internal heat integration. In the rectifying section, the majority of the heat duty is concentrated in the upper stages, especially in the condenser area. Notably, a large amount of heat is also rejected from stage R31, which is attributed to the introduction of superheated vapor into the system.

To identify effective heat exchange stages, it is necessary to calculate the $\varepsilon_{R,j}$ and $\varepsilon_{S,j}$. This study considers three different values for Q_E: 0.5, 1.0, and 1.5 times $\Delta H_{R,j}$ and $\Delta H_{S,j}$. Table 1 presents the impact of adding a single side reboiler at each stripper stage, showing how it affects main condenser and reboiler duties, as well as compression work W and inter-stage cooling duty Q_{int}. For the rectifying section, as shown in Table 2, only stages R2, R3, and R31 are considered for side condenser replacement, as they contribute over 5% of the total condenser heat duty. However, since stages R2 and R3 are located close to the main condenser R1, they operate at similar temperatures, providing minimal benefit over using the main condenser alone. Note that the $\varepsilon_{R,2}$ surpasses 100% even with $Q_E = 1.5 \cdot \Delta H_{R,j}$, which is caused by some nonlinear behaviors in distillation column.[54] Stage

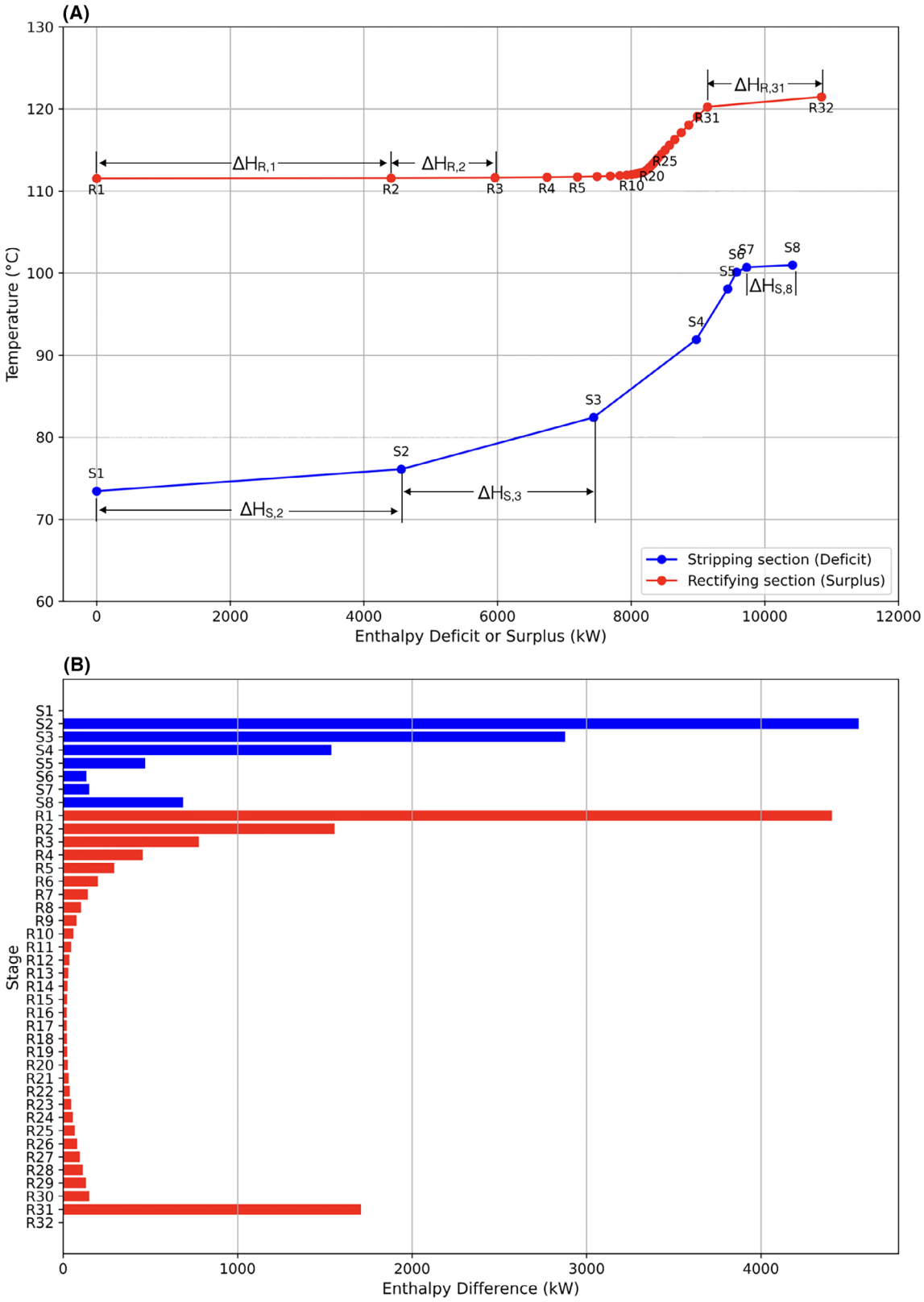

FIGURE 6 (A) CGCC for the high-pressure rectifying section and the low-pressure stripping section; (B) Enthalpy difference of each stage in both column sections.

TABLE 1 Effect of single-side reboiler in the stripping section.

Stage	Q_E (kW)	Q_R (kW)	ΔQ_R (kW)	$\varepsilon_{S,j}$	W (kW)	ΔW (kW)	$\Delta W/W_0$	Q_{int} (kW)	ΔQ_{int} (kW)	$\Delta Q_{\text{int}}/Q_{\text{int},0}$	Q_C (kW)	ΔQ_C (kW)	$\Delta Q_C/Q_{C,0}$
$Q_E = 0.5 \cdot \Delta H_{S,j}$													
S2	2279.96	8221.51	2191.69	96.13%	2048.83	11.70	0.57%	603.30	19.18	3.28%	10,927.40	80.04	0.74%
S3	1438.385	9004.44	1408.76	97.94%	2041.07	3.93	0.19%	590.59	6.48	1.11%	10,874.51	27.15	0.25%
S4	768.8	9654.31	758.89	98.71%	2038.44	1.30	0.06%	586.30	2.19	0.37%	10,855.94	8.58	0.08%
S5	235.025	10,180.30	232.90	99.10%	2037.42	0.28	0.01%	584.56	0.45	0.08%	10,849.66	2.30	0.02%
S6	66.38	10,347.36	65.84	99.19%	2037.22	0.08	0.00%	584.20	0.09	0.02%	10,848.20	0.84	0.01%
S7	74.45	10,338.97	74.23	99.70%	2037.16	0.03	0.00%	584.16	0.04	0.01%	10,847.51	0.15	0.00%
$Q_E = 1.0 \cdot \Delta H_{S,j}$													
S2	4559.92	6108.43	4304.77	94.40%	2070.58	33.44	1.64%	638.96	54.85	9.39%	11,081.18	233.82	2.16%
S3	2876.77	7610.60	2802.60	97.42%	2047.00	9.86	0.48%	600.21	16.09	2.75%	10,914.92	67.56	0.62%
S4	1537.6	8898.05	1515.15	98.54%	2040.14	3.01	0.15%	588.98	4.87	0.83%	10,867.81	20.45	0.19%
S5	470.05	9947.72	465.48	99.03%	2037.78	0.64	0.03%	585.04	0.93	0.16%	10,851.82	4.46	0.04%
S6	132.76	10,280.80	132.40	99.73%	2037.15	0.01	0.00%	584.25	0.14	0.02%	10,847.02	−0.34	0.00%
S7	148.9	10,264.45	148.75	99.90%	2037.13	0.00	0.00%	584.19	0.07	0.01%	10,847.25	−0.11	0.00%
$Q_E = 1.5 \cdot \Delta H_{S,j}$													
S2	6839.88	4226.69	6186.51	90.45%	2123.00	85.86	4.21%	718.37	134.25	22.98%	11,452.61	605.25	5.58%
S3	4315.155	6243.50	4169.70	96.63%	2056.39	19.25	0.95%	615.52	31.40	5.38%	10,980.91	133.55	1.23%
S4	2306.4	8144.38	2268.82	98.37%	2042.16	5.02	0.25%	592.26	8.14	1.39%	10,881.69	34.33	0.32%
S5	705.075	9714.72	698.48	99.06%	2038.03	0.89	0.04%	585.52	1.41	0.24%	10,853.36	6.00	0.06%
S6	199.14	10,215.20	198.01	99.43%	2037.29	0.15	0.01%	584.36	0.24	0.04%	10,848.64	1.28	0.01%
S7	223.35	10,190.10	223.10	99.89%	2037.14	0.00	0.00%	584.22	0.11	0.02%	10,847.23	−0.13	0.00%

TABLE 2 Effect of single side condenser in the rectifying section.

Stage	Q_E (kW)	Q_C (kW)	ΔQ_C (kW)	$\varepsilon_{R,j}$	W (kW)	ΔW (kW)	$\Delta W/W_0$	Q_{int} (kW)	ΔQ_{int} (kW)	$\Delta Q_{int}/Q_{int,0}$	Q_R (kW)	ΔQ_R(kW)	$\Delta Q_R/Q_{R,0}$
$Q_E = 0.5 \cdot \Delta H_{R,j}$													
R2	780.895	10,065.86	781.50	100.08%	2037.08	−0.06	0.00%	584.10	−0.01	0.00%	10,412.95	−0.25	0.00%
R3	390.615	10,458.52	388.84	99.55%	2037.55	0.41	0.02%	584.21	0.10	0.02%	10,415.07	1.87	0.02%
R31	840.37	10,712.27	135.09	16.08%	2172.60	135.46	6.65%	615.22	31.11	5.33%	11,014.44	601.24	5.77%
$Q_E = 1.0 \cdot \Delta H_{R,j}$													
R2	1561.79	9285.45	1561.91	100.01%	2037.12	−0.02	0.00%	584.11	0.00	0.00%	10,413.13	−0.07	0.00%
R3	781.23	10,070.88	776.48	99.39%	2038.09	0.96	0.05%	584.34	0.22	0.04%	10,417.47	4.27	0.04%
R31	1680.74	10,603.32	244.04	14.52%	2312.62	275.48	13.52%	647.14	63.02	10.79%	11,636.63	1223.43	11.75%
$Q_E = 1.5 \cdot \Delta H_{R,j}$													
R2	2342.685	8504.05	2343.31	100.03%	2037.08	−0.06	0.00%	584.10	−0.01	0.00%	10,412.95	−0.25	0.00%
R3	1171.845	9683.99	1163.37	99.28%	2038.75	1.62	0.08%	584.49	0.37	0.06%	10,420.40	7.20	0.07%
R31	2521.11	10,510.37	336.99	13.37%	2455.85	418.72	20.55%	679.53	95.42	16.34%	12,273.69	1860.49	17.87%

R31 is far from the overhead condenser, so $\varepsilon_{R,31}$ is very low. It is not beneficial to use the high-temperature heat here as it increases dramatically the compression work.

The analysis reveals that $\varepsilon_{R,j}$ and $\varepsilon_{S,j}$ are lower at certain stage due to significant temperature and composition differences between adjacent vapor and liquid flows. This indicates high thermodynamic irreversibility at these stages, meaning that energy losses are more substantial. Thus, $\varepsilon_{R,j}$ and $\varepsilon_{S,j}$ values can reflect the thermodynamic irreversibility at each stage. When thermodynamic irreversibility is low, the energy penalty is reduced, making these stages ideal for heat integration.

3.3 | Final design of D-HIDiC

3.3.1 | D-HIDiC with only external heat integration

The final design of D-HIDiC is developed based on the preliminary design results. As with the CDiC, the Sulzer standard Mellapak 350Y packing is chosen for the column internals, which reduces pressure drops compared with the preliminary design.

Design no. 1 (shown in Figure 7A) is based on the layout in Figure 4. This setup requires a heat exchanger and a loop to connect the compressed vapor with the column liquid. Two heat integration options can be considered:

- *Pumparound loop*: Liquid is drawn from the column, sent through a pump to a liquid–vapor heat exchanger to be heated (no vaporization due to the selected pump discharge pressure) and then returned to the column through a valve, flashing the hot liquid to column pressure.
- *Side reboiler*: Liquid is drawn from the column and fed into a thermosiphon side reboiler, which is heated by the compressed vapor.

In this case, the pumparound option is chosen as the more practical solution, as the inter-stage cooling is sensible heat with a large temperature change and thus adequate to heat a liquid (also sensible heat thus large temperature difference).

With low-pressure-drop packing, the simulated energy duties are slightly altered. The original condenser duty is now $Q_{C,0} = 10{,}821$ kW, the original reboiler duty $Q_{R,0} = 10{,}425$ kW, the total compression duty $W = 1986$ kW, and the inter-stage cooling duty $Q_{int} = 583$ kW.

In this pumparound configuration, liquid is drawn from stage S2 of the stripping section and pumped to 2.5 bar. It then exchanges heat with the compressed vapor, with an LMTD of 39.3°C. Here, $Q_E = 0.129 \cdot \Delta H_{S,2}$. After the heat integration via pumparound loop, the $Q_R = 9855$ kW, so the effectiveness factor $\varepsilon_{S,2} = (10{,}425 - 9855)/587 = 97.10\%$, indicating highly effective heat integration. The standard COP is defined as the ratio between the amount of heat upgraded (Q_b) and the heat pump energy requirement (W): $\mathrm{COP}_{std} = Q_b/W$.[6] In this case, the heat upgraded is calculated as $Q_b = 9855 + 587 = 10{,}442$ kW. The total compression duty increases slightly to $W = 1989$ kW after the intercooling heat recovery. Therefore, the $\mathrm{COP}_{\#1,std} = 10{,}442/1989 = 5.250$.

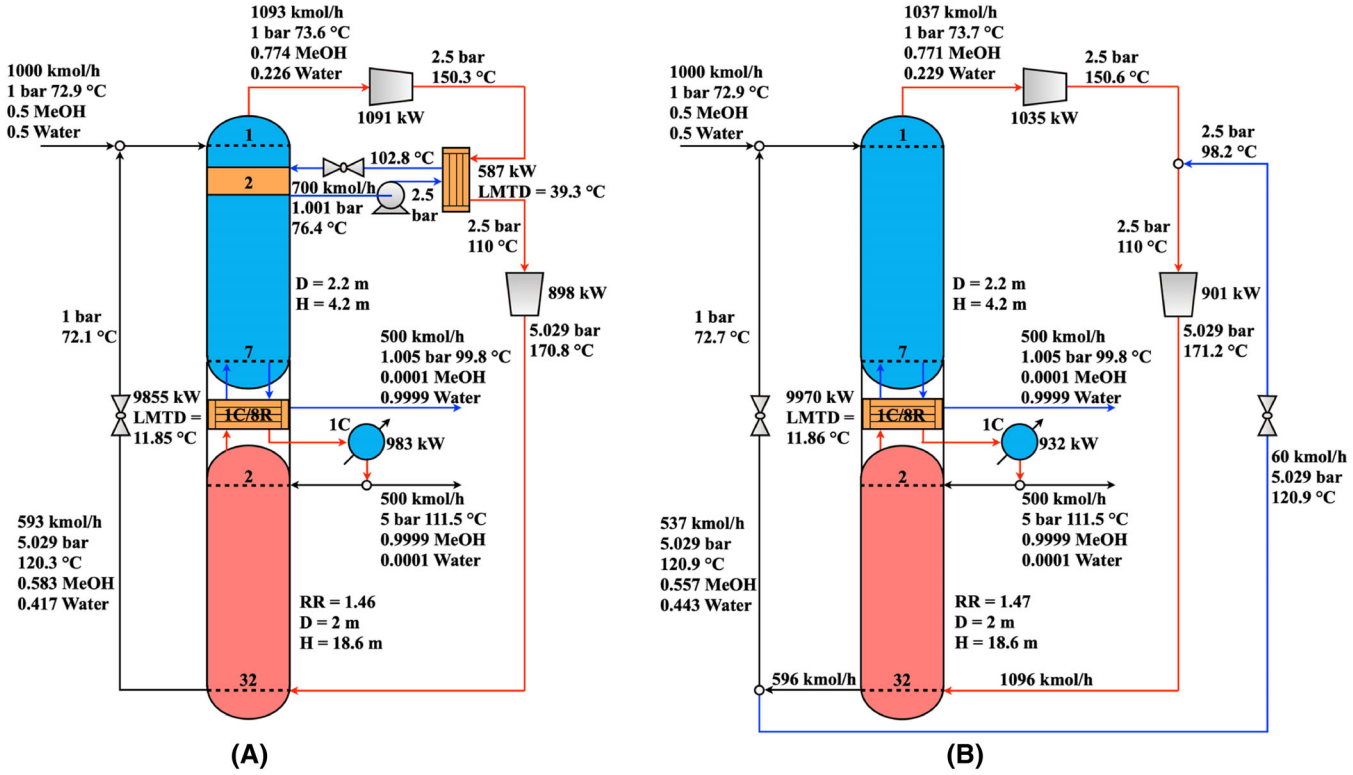

FIGURE 7 (A) D-HIDiC with pumparound loop (Design *no.* 1); (B) D-HIDiC with liquid injection (Design *no.* 2).

Design no. 2 (shown in Figure 7B) follows the liquid injection method illustrated in Figure 5. With low-pressure-drop packings, the energy duties are again adjusted slightly compared with the corresponding preliminary design. In this final design, external heat integration is the only consideration. The total compression duty is slightly reduced to 1936 kW, and the $COP_{\#2,std} = 9970/1936 = 5.150$.

It is noteworthy that $COP_{\#1,std} > COP_{\#2,std}$, yet the *Design no. 2* demonstrates better performance, as it uses 2.7% less compression power compared with *Design no. 1*. This counter-intuition arises because the calculation of heat upgraded in *Design no. 1* considers only the quantity of heat without distinguishing temperature levels—the direct sum of saved reboiler duty (~100°C) and stage heating (~76°C) is not an appropriate metric. To resolve this inconsistency, a modified COP can be defined to ensure a consistent evaluation of performance. A straightforward approach is to consider $Q_b = 10{,}078$ kW, representing the total heat usage in low-pressure CDiC (Figure 3A). Since the goal of designing D-HIDiC is to effectively achieve power-to-heat conversion, this approach aligns with the intended purpose. Under this circumstance, $COP_{\#1,mod} = 5.067$ and $COP_{\#2,mod} = 5.206$. These modified COP values intuitively show that *Design no. 2* is more effective in heat integration than *Design no. 1*. In addition, these designs serve as benchmarks for the subsequent stage-by-stage internal heat integration cases.

3.3.2 | D-HIDiC with both external and internal heat integration

Based on *Designs no. 1* and *no. 2*, we further explore configurations that incorporate both external and internal heat integration. As the stripping section is located above the rectifying section, the heat exchange can be accomplished by thermosiphon effect and gravity.[31]

Design no. 3 builds on *Design no. 1* by adding internal heat integration. In this configuration, stage R2 provides high-temperature heat to stage S3, as stage S2 has already been integrated with inter-stage cooling. Figure 8A shows this process configuration. In *Design no. 3*, the combined effectiveness of stage S2 and S3 is calculated as $\varepsilon_{S,2+3} = (10{,}425 - 7583)/(607 + 2343) = 96.34\%$ and for stage R2 $\varepsilon_{R,2} = (10{,}821 - 7583 - 995)/2343 = 95.73\%$. These values indicate effective internal heat integration. The total heat upgraded is calculated as $Q_b = 7583 + 2343 + 607 = 10{,}533$ kW and the total compression work is $W = 1098 + 903 = 2001$ kW. These values are higher than those in *Design no. 1*. However, the $COP_{\#3,std} = 5.264$, which is slightly higher than $COP_{\#1,std} = 5.250$. Despite the higher standard COP, this does not indicate better performance in terms of compression power usage. On the other hand, the $COP_{\#3,mod} = 5.036$ is lower than $COP_{\#1,mod} = 5.067$, which indicated the modified COP is a better performance indicator.

Design no. 4 is an improvement of *Design no. 2*, as shown in Figure 8B. Likewise, stages S3 and R2 are heat integrated.

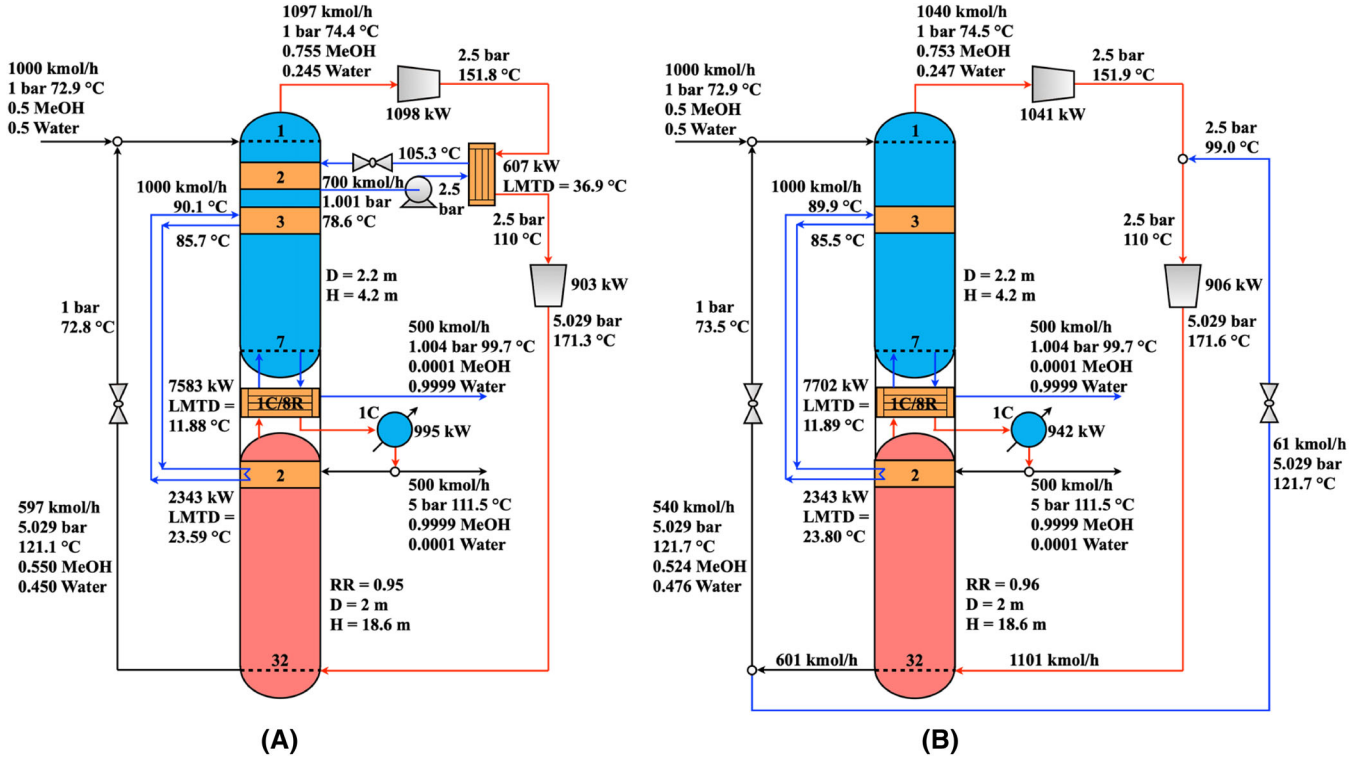

FIGURE 8 (A) D-HIDiC with pumparound loop and internal heat integration (Design *no*. 3); (B) D-HIDiC with liquid injection and internal heat integration (Design *no*. 4).

The effectiveness factors are $\varepsilon_{S,3} = (9970 - 7702)/2343 = 96.80\%$ and $\varepsilon_{R,3} = (10{,}902 - 7702 - 942)/2343 = 96.37\%$. These values also demonstrate good heat integration efficiency. The $COP_{\#4,std} = (7702 + 2343)/(1041 + 906) = 5.159$, which is higher than $COP_{\#2,std} = 5.150$, but *Design no. 4* uses more compression power. However, $COP_{\#4,mod} = 5.176$ is lower than $COP_{\#2,mod} = 5.206$. This comparison further highlights that the modified COP is a more reliable metric for evaluating process performance.

It should be noted that while internal heat integration improves heat distribution within the column, it does not reduce the total electricity input; it merely shifts some heat from the main condenser/reboiler to the side condenser/side reboiler, benefiting from a larger LMTD. However, *Designs no. 3* and *no. 4* use slightly more electricity than *Designs no. 1* and *no. 2*, respectively, due to a minor energy penalty associated with internal heat integration. Therefore, the simpler *Designs no. 1* and *no. 2* offer a better distillation electrification solution. In addition, both *Designs no.1* and *no.2* also exhibit favorable dynamic controllability under varying operating conditions.[55]

4 | EVALUATION OF ENERGY CONSERVATION OF D-HIDiC

The energy use of the D-HIDiC design options with either pumparound loops or liquid injection is compared with that of other configurations, including the CDiC, C-HIDiC, and SuperHIDiC. As *Design no. 2* has the lowest compression power usage, the liquid injection design will also be considered in C-HIDiC and SuperHIDiC. For consistency in the comparison, the feedstock, column internals, and separation specifications are kept identical across all processes.

4.1 | CDiC

Using the low-pressure CDiC (Figure 3A) as a benchmark, the reboiler duty is 10,078 kW. In terms of energy quantity, *Design no. 2* achieves a significant energy saving of 80.8% compared with the CDiC. When the electrical power consumption is converted into primary fuel energy with 36.6% power generation efficiency,[56] the primary energy savings provided by *Design no. 2* amount to 47.5%.

4.2 | C-HIDiC

As a comparison to the D-HIDiC processes, a C-HIDiC with continuous heat exchange is considered in *Design no. 5*. *Design no. 2* is used as the benchmark for this evaluation, as it does not involve integrating intercooling duty within the stripping column. In the C-HIDiC, the rectifying and stripping sections are installed in parallel, with internal heat exchangers physically implemented between stages at the same level.

For a conservative design, a heat transfer coefficient of $0.5\,kW\,m^{-2}\,K^{-1}$ is assumed, and a uniform heat transfer area of $80\,m^2$ per stage is used for the stage-by-stage heat integration.[57] This design ensures stable distillation operation, as excessive heat transfer could dry out the column, causing a lack of vapor in the top section of the

rectifying column. Table 3 lists the heat transfer locations and corresponding heat exchange duties.

The simulation results are outlined in Figure 9. In the C-HIDiC (Figure 1A), there is typically no heat integration between the main condenser and the main reboiler. However, deliberate heat integration between them is implemented to maximize energy utilization, allowing the process to be fully electrified.

The total internal heat exchange duty is 6426 kW, while the external heat exchange duty is 4015 kW. The effectiveness factors are $\varepsilon_{S,1-7} = (9970 - 4015)/6426 = 92.67\%$ and $\varepsilon_{R,2-8} = (10{,}902 - 4015 - 1006)/6426 = 91.52\%$, and thus introducing large energy penalties. In summary, these effectiveness factors indicate that the total heat exchange duty and compression duty in *Design no. 5* increase by 4.7% and 4.0%, respectively, compared with *Design no. 2*. Likewise, the increased $COP_{\#5,std} = 5.187$ does not reflect a better performance. Table 4 provides an overview of the heat exchanger areas (excluding the condenser area) and energy utilization for different designs. As observed, higher heat transfer rates result in lower effectiveness factor. However, they also reduce the required heat exchanger area, demonstrating a trade-off between energy consumption and equipment sizing.

4.3 | SuperHIDiC

The commercially operated D-HIDiC, also known as SuperHIDiC (www.toyo-eng.com/jp/en/solution/superhidic/), is detailed in the US patent (US 2012/0125761) with Toyo Engineering Corporation as the assignee. The SuperHIDiC proposed by Wakabatashi et al.[28] is different from the one proposed in this work. Instead of relying solely on

TABLE 3 Heat transfer rate on each column stage.

Rectifying section stage	Rectifying section stage temperature (°C)	Stripping section stage	Stripping section stage temperature (°C)	Temperature difference (°C)	Heat exchanging duty (kW)
R2	111.57	S1	73.72	37.85	1514
R3	111.58	S2	76.27	35.30	1412
R4	111.59	S3	82.49	29.10	1164
R5	111.60	S4	91.68	19.92	797
R6	111.61	S5	97.47	14.13	565
R7	111.62	S6	99.25	12.37	495
R8	111.63	S7	99.66	11.97	479

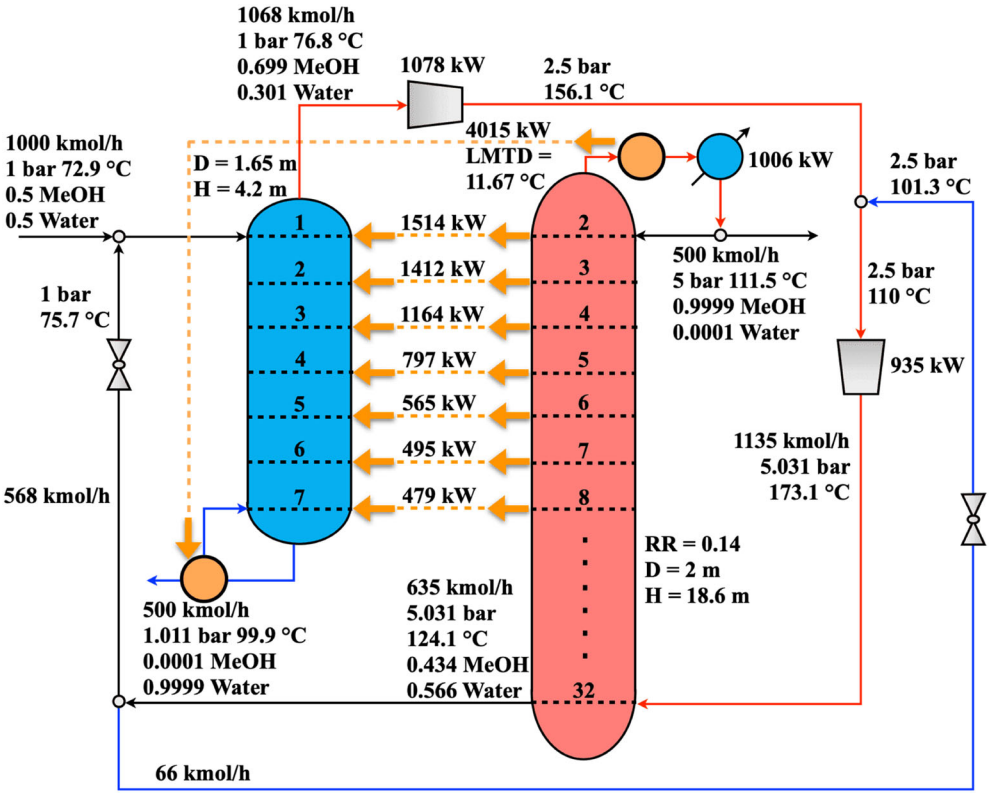

FIGURE 9 C-HIDiC with continuous heat exchanging (Design *no.* 5).

hot vapor from the top of the rectifying section to drive the main reboiler, as in this work, the Japanese SuperHIDiC integrates three side reboilers in the low-pressure stripping section, with heat sourced from the hot vapor. Our analysis suggests that the introduction of side reboilers can lead to energy penalties. Side reboilers positioned higher in the stripping section generally face greater energy penalties due to reduced separation driving force. However, these positions also offer greater temperature differences, thus improving heat transfer efficiency. This trade-off highlights the balance between energy penalties and temperature differences available for heat integration. In the SuperHIDiC, the main reboiler is driven by compressed stripping section overhead vapor, which is delivered to the main reboiler located at the bottom of the stripping section. The condensate is sent to the bottom of the high-pressure rectifying section, where it flashes, generating the necessary boilup flow.

Based on *Design no. 2*, a process simulation was performed to evaluate the effect of using the compressed stripping section overhead vapor to partially drive one of the main reboilers, while maintaining a liquid fraction of 0.15 in the outlet stream. The remaining duty is handled by the main condenser. This design option is named *Design no. 6*, and Figure 10A shows the results. Although the compressed vapor can drive one of the main reboilers at a higher temperature difference, the associated energy penalty is substantial. The total compression power increases to 2410 kW, ~20% higher than the original *Design no. 2*. Additionally, the main reboiler duty rises to 12,090 kW (a 17.5% increase compared with *Design no. 2*), while the main condenser duty decreases slightly to 10,611 kW (compared with the original 10,902 kW). These results indicate that directly utilizing compressed stripping section overhead vapor to heat the stripping column is not an effective option for D-HIDiC design, at least for the methanol/water case.

TABLE 4 Heat exchanger area and energy utilization for different designs.

	Design no. 1	Design no. 2	Design no. 3	Design no. 4	Design no. 5	Design no. 6	Design no. 7
Heat exchange duty (kW)	10,442	9970	10,533	10,045	10,441	12,090	10,049
Number of heat exchanger	3	2	4	3	8	3	2
Heat exchanger area (m^2)	1693	1681	1508	1492	1248	1795	1769
Compression power (kW)	1989	1936	2001	1947	2013	2410	2006
COP_{std}	5.250	5.150	5.264	5.159	5.187	5.017	5.009
COP_{mod}	5.067	5.206	5.036	5.176	5.006	4.182	5.024

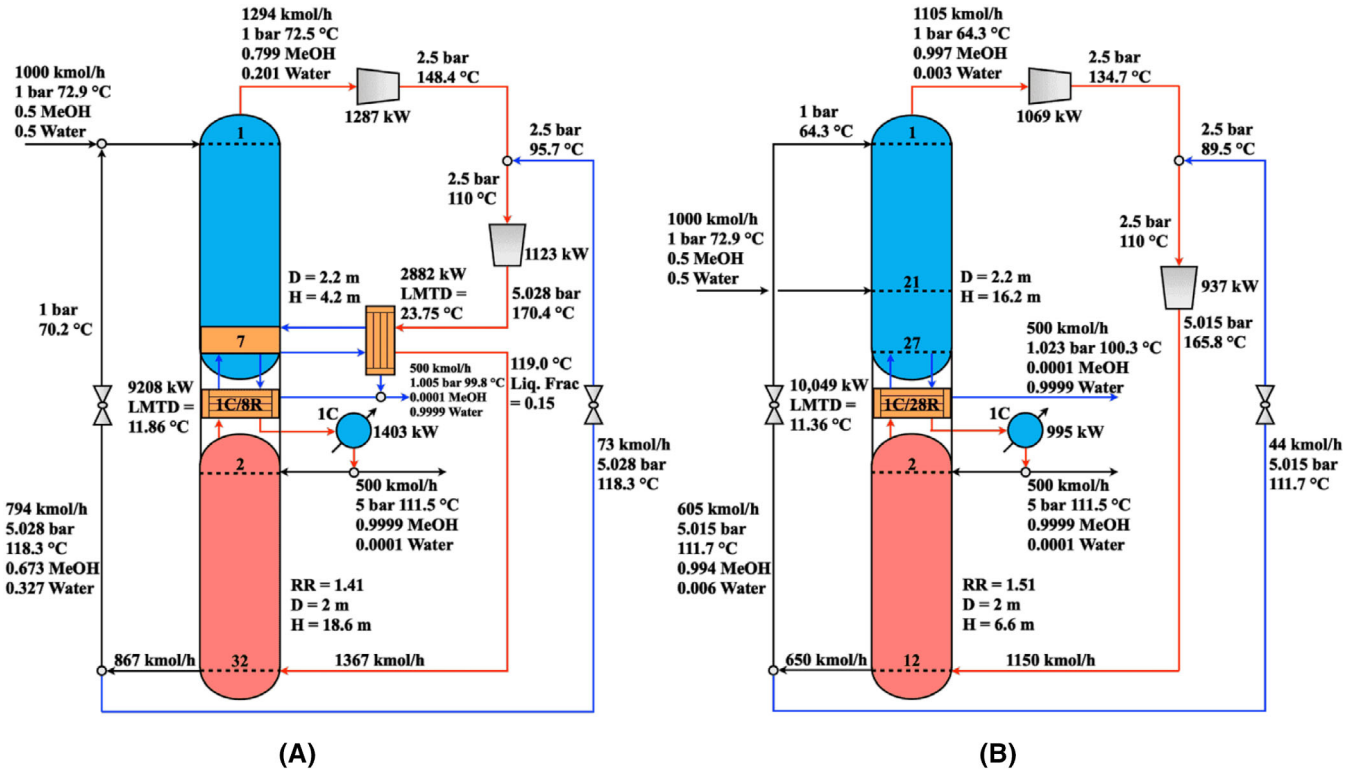

FIGURE 10 SuperHIDiC with (A) driving column by compressed stripping section overhead vapor (Design no. 6) and (B) moving high-pressure rectifying section to low-pressure section (Design no. 7).

Another key point of the SuperHIDiC design involves relocating the lower part of the rectifying section to low-pressure section, leveraging higher relative volatility at lower pressure. To evaluate this *Design no. 7*, we modified the stage distribution of *Design no. 2* by transferring 20 stages from the high-pressure column to the low-pressure column. In such case, the low-pressure column now has 28 stages, and the high-pressure column has 12 stages. The feed stage is at stage 21 in low-pressure column. Figure 10B shows the simulation results. The stripping overhead vapor now achieves high methanol purity, indicating sufficient separation stages, thus the higher relative volatility has limited effect on saving energy consumption. The overall compression power is 2006 kW, higher than the original 1936 kW. Thus, modifying the feed stage does not offer any advantage in this methanol/water distillation scenario.

5 | CONCLUSIONS

This work proposes several new D-HIDiC design options, evaluated systematically using Aspen Plus without rigorous process optimization. By creatively integrating external and internal heat exchange mechanisms, we examined configurations ranging from simple designs with only external heat integration to more complex ones incorporating both external and internal heat integration. The novel utilization of liquid injection technology, exemplified in *Design no. 2*, represents a significant advancement over conventional pumparound loops (*Design no. 1*). This configuration stands out due to its exceptional balance between simplicity and energy efficiency. Specifically, *Design no. 2* achieves approximately 50% primary energy savings compared with CDiC for methanol/water separation, underscoring its practical value for industrial-scale electrification. Although internal heat integration approaches (*Designs no. 3*, *no. 4*, and *no. 5*) offer opportunities for improved heat redistribution, the additional complexity and higher electricity consumption limit their practical advantage. Similarly, attempts to implement SuperHIDiC principles (*Designs no. 6* and *no. 7*) show no clear benefits over the optimal external integration configuration (*Design no. 2*).

Overall, the innovations presented—particularly the introduction and validation of liquid injection for effective intercooling heat recovery—significantly extend the applicability of HIDiC systems to separations with larger boiling point differences. This work makes a meaningful contribution toward the broader goal of electrifying industrial distillation processes, enhancing energy efficiency, and reducing environmental impacts.

Future research should build upon these findings by investigating rigorous optimization strategies, experimental validations, and potential scalability to more complex, real-world mixtures.

AUTHOR CONTRIBUTIONS

Chengtian Cui: Conceptualization; methodology; software; data curation; validation; visualization; writing – original draft; writing – review and editing. **Jos van Reisen:** Methodology; formal analysis; data curation; validation; writing – review and editing. **Ioannis Tyraskis:** Methodology; formal analysis; validation; writing – review and editing. **Anton A. Kiss:** Conceptualization; methodology; formal analysis; investigation; funding acquisition; supervision; resources; project administration; writing – review and editing.

ACKNOWLEDGMENTS

This research was carried out within the REMAP2 project (TIND23-03473469) with a Top Sector Energy subsidy from the Ministry of Economic Affairs and Climate in The Netherlands.

DATE AVAILABILITY STATEMENT

Figures 1–5 and 7–10 are graphical representations of process flowsheets or conceptual designs, so there is no numerical data associated with them. Numerical data supporting Figures 6 and S1 can be found in the "Supporting Data" Excel file. Aspen Plus simulation files are available upon reasonable request.

ORCID

Anton A. Kiss https://orcid.org/0000-0001-5099-606X

REFERENCES

1. Sholl DS, Lively RP. Seven chemical separations to change the world. *Nature*. 2016;532(7600):435-437. doi:10.1038/532435a
2. Kiss AA, Smith R. Rethinking energy use in distillation processes for a more sustainable chemical industry. *Energy*. 2020;203:117788. doi:10.1016/j.energy.2020.117788
3. Mekidiche Z, Labarta JA, Javaloyes-Anton J, Caballero JA. From power to heat: strategies for electrifying distillation for sustainable chemical processes. *Appl Therm Eng*. 2024;257:124316. doi:10.1016/j.applthermaleng.2024.124316
4. Cui C, Qi M, Zhang X, et al. Electrification of distillation for decarbonization: an overview and perspective. *Renew Sustain Energy Rev*. 2024;199:114522. doi:10.1016/j.rser.2024.114522
5. Adami M, Farheen K, Skiborowski M. Electrifying distillation – optimization-based evaluation of internally heat-integrated distillation columns. *Sep Purif Technol*. 2025;360:131061. doi:10.1016/j.seppur.2024.131061
6. Kiss AA. *Advanced Distillation Technologies: Design, Control and Application*. John Wiley & Sons; 2013.
7. Kiss AA, Flores Landaeta SJ, Infante Ferreira CA. Towards energy efficient distillation technologies – making the right choice. *Energy*. 2012;47(1):531-542. doi:10.1016/j.energy.2012.09.038
8. Jana AK. Advances in heat pump assisted distillation column: a review. *Energ Conver Manage*. 2014;77:287-297. doi:10.1016/j.enconman.2013.09.055
9. Wang H, Yu P, Chen L, Chen L, Sun B. Simulation and modification of an ethane-ethylene separation unit using vapor recompression heat pump: energy, exergy, and economic analyses. *Appl Therm Eng*. 2024;239:121993. doi:10.1016/j.applthermaleng.2023.121993
10. Leo MB, Dutta A, Farooq S. Process synthesis and optimization of heat pump assisted distillation for ethylene-ethane separation. *Ind Eng Chem Res*. 2018;57(34):11747-11756. doi:10.1021/acs.iecr.8b02496
11. Christopher CCE, Dutta A, Farooq S, Karimi IA. Process synthesis and optimization of propylene/propane separation using vapor recompression and self-heat recuperation. *Ind Eng Chem Res*. 2017;56(49):14557-14564. doi:10.1021/acs.iecr.7b03432
12. Kazemi A, Mehrabani-Zeinabad A, Beheshti M. Novel heat pump assisted distillation configurations for energy and economic savings and their application on propylene/propane and I-butane/N-butane

separation systems. *Chem Eng Sci*. 2024;295:120139. doi:10.1016/j.ces.2024.120139

13. Cui C, Zhang X, Qi M, Lyu H, Sun J, Kiss AA. Fully electrified heat pump assisted distillation process by flash vapour circulation. *Chem Eng Res Des*. 2024;206:280-284. doi:10.1016/j.cherd.2024.05.011
14. Qi M, Zhang X, Wong DS, Shu C, Cui C, Kiss AA. Electrified distillation with flash vapor circulation and thermal storage for dynamic electricity markets. *AIChE J*. 2025;71(5):e18750. doi:10.1002/aic.18750
15. Cui C, Long NVD, Sun J, Lee M. Electrical-driven self-heat recuperative pressure-swing azeotropic distillation to minimize process cost and CO_2 emission: process electrification and simultaneous optimization. *Energy*. 2020;195:116998. doi:10.1016/j.energy.2020.116998
16. Navarro-Amorós MA, Ruiz-Femenia R, Caballero JA. A new technique for recovering energy in thermally coupled distillation using vapor recompression cycles. *AIChE J*. 2013;59(10):3767-3781. doi:10.1002/aic.14137
17. Duanmu F, Sorensen E. Optimal design of reduced vapor transfer dividing wall structures with and without heat integration. *AIChE J*. 2024;70(11):e18572. doi:10.1002/aic.18572
18. Kiss AA, Olujić Ž. A review on process intensification in internally heat-integrated distillation columns. *Chem Eng Process*. 2014;86:125-144. doi:10.1016/j.cep.2014.10.017
19. Shahandeh H, Jafari M, Kasiri N, Ivakpour J. Economic optimization of heat pump-assisted distillation columns in methanol-water separation. *Energy*. 2015;80:496-508. doi:10.1016/j.energy.2014.12.006
20. De Rijke A. Development of a Concentric Internally Heat Integrated Distillation Column (HIDiC). PhD Thesis. Delft University of Technology, Delft, the Netherlands. 2007.
21. Bruinsma OSL, Tromp SA, Strijker M, et al. *Heat Integrated Distillation Using a Plate-Fin Heat Exchanger*. CHISA; 2010.
22. Bruinsma OSL, Krikken T, Cot J, et al. The structured heat integrated distillation column. *Chem Eng Res Des*. 2012;90(4):458-470. doi:10.1016/j.cherd.2011.08.023
23. Luyben WL. Energy management in distillation preheat systems. *Chem Eng Process*. 2020;156:108074. doi:10.1016/j.cep.2020.108074
24. Kansha Y, Kishimoto A, Tsutsumi A. Process design methodology for high-energy saving HIDiC based on self-heat recuperation. *Asia-Pacific J Chem Eng*. 2011;6(3):320-326. doi:10.1002/apj.582
25. Sun S, Yang A, Chien I-L, et al. Intensification and performance assessment for synthesis of 2-methoxy-2-methyl-heptane through the combined use of different pressure thermally coupled reactive distillation and heat integration technique. *Chem Eng Process*. 2019;142:107561. doi:10.1016/j.cep.2019.107561
26. Liu L, Zhu L, Sun L, Zhu M, Liu G. Simulation and optimization of different pressure thermally coupled distillation for separating a close-boiling mixture of n-butanol and iso-butanol. *Appl Petrochem Res*. 2017;7(2–4):143-150. doi:10.1007/s13203-017-0186-1
27. Sun L, He K, Liu Y, Wang Q, Wang D. Analysis of different pressure thermally coupled extractive distillation column. *Open Chem Eng J*. 2014;8(1):12-18. doi:10.2174/1874123101408010012
28. Wakabayashi T, Yoshitani K, Takahashi H, Hasebe S. Verification of energy conservation for discretely heat integrated distillation column through commercial operation. *Chem Eng Res Des*. 2019;142:1-12. doi:10.1016/j.cherd.2018.11.031
29. Wakabayashi T, Ferrari A, Hasebe S. Design and commercial operation of a discretely heat-integrated distillation column. *Chem Eng Res Des*. 2019;147:214-221. doi:10.1016/j.cherd.2019.04.036
30. Wakabayashi T, Hasebe S. Design of heat integrated distillation column by using H-Xy and T-Xy diagrams. *Comput Chem Eng*. 2013;56:174-183. doi:10.1016/j.compchemeng.2013.05.020
31. Wakabayashi T, Hasebe S. Higher energy saving with new heat integration arrangement in heat-integrated distillation column. *AIChE J*. 2015;61(10):3479-3488. doi:10.1002/aic.14865
32. Harwardt A, Marquardt W. Heat-integrated distillation columns: vapor recompression or internal heat integration? *AIChE J*. 2012;58(12):3740-3750. doi:10.1002/aic.13775
33. Shenvi AA, Herron DM, Agrawal R. Energy efficiency limitations of the conventional heat integrated distillation column (HIDiC) configuration for binary distillation. *Ind Eng Chem Res*. 2011;50(1):119-130. doi:10.1021/ie101698f
34. Herrera Velázquez JJ, Zavala Durán FM, Chávez Díaz LA, Cabrera Ruiz J, Alcántara Avila JR. Hybrid two-step optimization of internally heat-integrated distillation columns. *J Taiwan Inst Chem Eng*. 2022;130:103967. doi:10.1016/j.jtice.2021.06.061
35. Rix A, Paul N, Wessner L, Murrenhoff D. Optimization of heat pump and vapor recompression Technologies for Wide-Boiling Mixtures. In: Manenti F, Reklaitis GV, eds. *Book of Abstract of the 34th European Symposium on Computer Aided Process Engineering / 15th International Symposium on Process Systems Engineering (ESCAPE34/PSE24)*. IEEE; 2024:275-280.
36. Kiss AA, Pragt JJ, Vos HJ, Bargeman G, de Groot MT. Novel efficient process for methanol synthesis by CO_2 hydrogenation. *Chem Eng J*. 2016;284:260-269. doi:10.1016/j.cej.2015.08.101
37. Vaquerizo L, Kiss AA. Thermally self-sufficient process for single-step coproduction of methanol and dimethyl ether by CO_2 hydrogenation. *J Clean Prod*. 2024;441:140949. doi:10.1016/j.jclepro.2024.140949
38. Luyben WL. Design and control of a methanol reactor/column process. *Ind Eng Chem Res*. 2010;49(13):6150-6163. doi:10.1021/ie100323d
39. Shen Z, Qu Q, Chen M, Lyu H, Sun J. Advancements in methanol distillation system: a comprehensive overview. *Chem Eng Res Des*. 2023;199:130-151. doi:10.1016/j.cherd.2023.09.026
40. Cui C, Li X, Sui H, Sun J. Optimization of coal-based methanol distillation scheme using process superstructure method to maximize energy efficiency. *Energy*. 2017;119:110-120. doi:10.1016/j.energy.2016.12.065
41. Cui C, Xi Z, Liu S, Sun J. An enumeration-based synthesis framework for multi-effect distillation processes. *Chem Eng Res Des*. 2019;144:216-227. doi:10.1016/j.cherd.2019.02.018
42. Caspari A, Offermanns C, Schäfer P, Mhamdi A, Mitsos A. A flexible air separation process: 1. Design and steady-state optimizations. *AIChE J*. 2019;65(11):e16705. doi:10.1002/aic.16705
43. Caspari A, Offermanns C, Schäfer P, Mhamdi A, Mitsos A. A flexible air separation process: 2. Optimal operation using economic model predictive control. *AIChE J*. 2019;65(11):e16721. doi:10.1002/aic.16721
44. Dhole VR, Linnhoff B. Distillation column targets. *Comput Chem Eng*. 1993;17(5–6):549-560. doi:10.1016/0098-1354(93)80043-M
45. Luyben WL. *Distillation Design and Control Using AspenTM Simulation*. John Wiley & Sons, Inc.; 2013. doi:10.1002/9781118510193
46. Rix A, Schröder M, Paul N. Vapor recompression: an interesting option for vacuum columns? *Chem Eng Res Des*. 2023;191:226-235. doi:10.1016/j.cherd.2023.01.030
47. Luo H, Bildea CS, Kiss AA. Novel heat-pump-assisted extractive distillation for bioethanol purification. *Ind Eng Chem Res*. 2015;54(7):2208-2213. doi:10.1021/ie504459c
48. Luyben WL. Compressor heuristics for conceptual process design. *Ind Eng Chem Res*. 2011;50(24):13984-13989. doi:10.1021/ie202027h
49. Reddy CCS, Fang Y, Rangaiah GP. Improving energy efficiency of distillation using heat pump assisted columns. *Asia-Pacific J Chem Eng*. 2014;9(6):905-928. doi:10.1002/apj.1842
50. Cui C, Qi M, Ni H, Fu J, Sun J. Intensifying petroleum fractionators through internal partial condensation in place of pump-around. *Fuel Process Technol*. 2022;231:107251. doi:10.1016/j.fuproc.2022.107251
51. Khan A, Bradshaw CR. Quantitative comparison of the performance of vapor compression cycles with compressor vapor or liquid

injection. *Int J Refrig*. 2023;154:386-394. doi:10.1016/j.ijrefrig.2023.07.012
52. Schmitt J, Langebach R. High-pressure liquid refrigerant injection for reciprocating compressors. *Int J Refrig*. 2024;164:29-37. doi:10.1016/j.ijrefrig.2024.04.017
53. Suphanit B. Optimal heat distribution in the internally heat-integrated distillation column (HIDiC). *Energy*. 2011;36(7):4171-4181. doi:10.1016/j.energy.2011.04.026
54. Yan L, Edgar TF, Baldea M. Dynamic process intensification of binary distillation based on output multiplicity. *AIChE J*. 2019;65(4):1162-1172. doi:10.1002/aic.16506
55. Cui C, Li Q, Luyben WL, Kiss AA. Dynamics and control of discretely heat integrated distillation columns. *Comput Chem Eng*. 2025:109144. doi:10.1016/j.compchemeng.2025.109144
56. Matsuda K, Kansha Y, Fushimi C, Tsutsumi A, Kishimoto A. *Advanced Energy Saving and Its Applications in Industry*. Springer London; 2013. doi:10.1007/978-1-4471-4207-2
57. Suphanit B. Design of internally heat-integrated distillation column (HIDiC): uniform heat transfer area versus uniform heat distribution. *Energy*. 2010;35(3):1505-1514. doi:10.1016/j.energy.2009.12.008

SUPPORTING INFORMATION

Additional supporting information can be found online in the Supporting Information section at the end of this article.

How to cite this article: Cui C, van Reisen J, Tyraskis I, Kiss AA. Efficient heat integration within discretely heat integrated distillation columns using liquid injection. *AIChE J*. 2025;71(8):e18861. doi:10.1002/aic.18861